Features of F_1-ATPase Catalytic and Noncatalytic Sites Revealed by Fluorescence Lifetimes and Acrylamide Quenching of Specifically Inserted Tryptophan Residues†

Joachim Weber* and Alan E. Senior

Department of Biochemistry and Biophysics, Box 712, University of Rochester Medical Center, Rochester, New York 14642

Received November 29, 1999; Revised Manuscript Received February 24, 2000

ABSTRACT: Catalytic and noncatalytic nucleotide sites of the F_1 sector of ATP synthase were characterized by tryptophan fluorescence techniques. Seven Trp residues inserted in varied microenvironments in the catalytic sites, and one in the noncatalytic sites, were studied in mutant F_1 enzymes which were otherwise devoid of Trp. Parameters measured were fluorescence lifetimes and dynamic and static quenching by acrylamide in the absence or presence of nucleotide. The results indicated that the solution structures of the mutant enzymes were consistent with reported crystal structures. In enzyme with three empty noncatalytic sites, all sites were relatively inaccessible to acrylamide, indicating a closed conformation. In contrast, when the three catalytic sites were empty, they were relatively and equally accessible to acrylamide, indicating an open conformation. This was the case in the presence or absence of Mg^{2+}. Residue β-Trp-331 has been extensively used previously to determine nucleotide binding parameters in F_1. Results here showed that in βY331W mutant F_1, each of the three β-Trp-331 residues has an unusually long fluorescence lifetime, confirming that each contributes equally to the overall fluorescence signal.

ATP synthase is the enzyme responsible for ATP synthesis in oxidative phosphorylation. F_1-ATPase (often called "F_1") is the catalytic portion of ATP synthase; it has the subunit stoichiometry $\alpha_3\beta_3\gamma\delta\epsilon$, and carries a total of six nucleotide binding sites. Three of these sites are catalytic sites which participate directly in ATP synthesis and ATP hydrolysis. X-ray structure analysis revealed that each of the catalytic sites is formed primarily by residues of a β-subunit, with some contributions from residues of the adjacent α-subunit (*1*). The remaining three sites, formed predominantly by residues of the three α-subunits (*1*), do not participate directly in catalysis, and in fact, all attempts to assign a clear-cut physiological function to these "noncatalytic sites" have failed so far (for recent reviews, see refs *2*, *3*).

To obtain probes capable of monitoring, on real-time basis, occupancy of the nucleotide binding sites by substrates, products, and nucleotide analogues, we have in recent years introduced by mutagenesis a number of Trp residues into the close proximity of the catalytic and noncatalytic sites in *Escherichia coli* F_1. The fluorescence responses of these Trp residues have been used to determine thermodynamic and kinetic ligand binding parameters of the two types of nucleotide site, and this experimental approach has led to a remarkable number of advances, for example, in formulating the catalytic cycle of ATP hydrolysis, in uncovering the role of Mg^{2+} ions in generation of asymmetry of the three catalytic sites, in elucidation of the structure of the catalytic transition state, in explaining the mechanism of action of inhibitors and inhibitory mutations, and in describing the characteristics of the noncatalytic sites (see refs *2*, *4*, *5* for reviews of this work).

Trp residues that we introduced previously to investigate properties of the catalytic sites were purposefully placed in a variety of unique locations relative to the position of the bound nucleotide, and their fluorescence spectra indicated that they occupied a range of different environments (Figure 6 of ref *6* displays the arrangement of Trp substitutions in *E. coli* F_1 catalytic sites; their steady-state fluorescence spectra are reported or referenced in that paper). It was apparent, therefore, that more information about the accessibility of the catalytic sites, and about conformational changes resultant from ligand binding, could be gained from these Trp substitutions by further exploiting the fluorescence technique. Thus, in this paper we describe first fluorescence lifetime measurements; then, in acrylamide quenching experiments, we assess the accessibility of several catalytic-site-located Trp residues and changes seen upon ligand binding. For comparison, we performed similar experiments with a Trp residue substituted in the noncatalytic sites. The results obtained give insights into the relative accessibility and conformation of the catalytic sites under different conditions, demonstrate clear differences between catalytic and noncatalytic sites, and indicate that when all three catalytic sites in intact F_1 are unoccupied, they each assume an "open" conformation, as in the X-ray structure of the $\alpha_3\beta_3$ complex (*7*).

EXPERIMENTAL PROCEDURES

Construction of Plasmids for Expression of Single Tryptophan Mutants in Otherwise Tryptophan-Free F_1 Background. (i) Construction of Plasmid pRLL2 Containing the βF176W Mutation with Replacements of All Naturally Occurring Trp Residues in F_1. Oligonucleotide-directed mutagenesis was used (*8*) to generate the βF176W[1] mutation. The template was M13mp18 containing the *Hin*D3−*Kpn*I

† Supported by NIH Grant GM25349 to A.E.S.

* Correspondence should be addressed to this author: 716-275-2920 phone, 716-271-2683 FAX, joachim_weber@urmc.rochester.edu e-mail.

10.1021/bi992730t CCC: $19.00
Published on Web 04/14/2000

fragment from plasmid p0W1. In p0W1, all naturally occurring Trp residues in F_1 have been replaced, to allow purification of Trp-free enzyme (*9*). The mutagenic oligonucleotide was T TAC TCT GTG T**GG** GC*C* GGC GTA GG in which the boldface bases encode the Phe to Trp substitution and the italicized base introduces a new *Ngo*MI site for identification of mutant clones. Mutant RF were identified, and DNA sequencing was carried out to confirm the presence of the new Trp codon and the absence of any undesired mutation. The βF176W mutation was then moved into plasmid p0W1 on an *Nhe*I−*Kpn*I fragment, yielding plasmid pRLL1. In recent work, it was shown that expression of mutant F_1 from plasmid pBWU13.4 in strain DK8 (*10, 11*) gives enhanced yield of enzyme. Therefore, the βF176W mutation was moved from pRLL1 into plasmid pBWU13.4 on a *Xho*I−*Eag*I fragment, to give plasmid pRLL1A. This manipulation also transferred four of the five natural Trp replacements present in p0W1, namely, αW513F/γW108Y/γW206Y/βW107F, into pRLL1A. The fifth natural Trp replacement (δW28L) was moved into pRLL1A from p0W1 on a *Ppu*MI−*Sph*I fragment. The final plasmid, named pRLL2, carries the βF176W mutation together with replacements of all Trp residues present naturally in F_1. It was transformed into strain DK8 (yielding pRLL2/DK8) for purification of βF176W enzyme.

(ii) Construction of Strains Carrying βF148W, βV153W, βY331W, βF410W, or αR365W Mutations in Otherwise Trp-Free F1. An *Xho*I−*Eag*I fragment was used to transfer the following mutations into plasmid pRLL2: βF148W mutation (from plasmid pCB1, ref *12*); βV153W (from plasmid pCB2, ref *12*); βY331W (from plasmid pCB5, ref *13*); αR365W (from plasmid pCB7, previously constructed by transferring a *Xho*I−*Bst*BI fragment from pAW7, ref *14*, into plasmid p0W1). For the βF410W mutation, an *Xho*I−*Sgf*I fragment containing the βF410W mutation in Trp-free background (plasmid pSWM50, ref *6*) was transferred into pRLL2. In each case, disappearance of the introduced *Ngo*MI site in pRLL2 was used to monitor successful transfer. The new plasmids were, respectively, pRLL3 (βF148W), pSWM80 (βV153W), pSWM81 (βY331W), pSWM82 (αR365W), and pSWM83 (βF410W). Each was transformed into strain DK8 for expression and F_1 purification. For purification of F_1 containing the mutations αF291W or αF354W, previously described strains (*6*) were used.

Enzyme Purification and Characterization. F_1 was purified according to ref *15*. αR365W mutant F_1 was depleted of endogenous nucleotides as described (*16*). Purity and subunit composition of F_1 preparations were checked by SDS-gel electrophoresis (*17*). Protein concentrations were determined using the Bio-Rad protein assay (*18*). Growth yield analyses in limiting glucose (3 mM) and tests of growth on succinate plates were carried out as described (*19*). Standard ATPase activities were assayed in 50 mM Tris/H_2SO_4, 10 mM ATP, and 4 mM $MgSO_4$, pH 8.5, at 30 °C. ATPase activity in the presence of acrylamide was determined using 50 mM Tris/H_2SO_4, 5 mM ATP, 2 mM $MgSO_4$, pH 8.0, plus the indicated concentration of acrylamide, at 23 °C. Dependence of enzyme activity on substrate concentration was measured in buffer containing 50 mM Tris/H_2SO_4, pH 8.0, with varying concentrations of ATP (0.02−10 mM) and $MgSO_4$ (0.008−4 mM) in a constant ratio of 2.5/1. Released P_i was determined by colorimetric assays (*20, 21*).

Fluorescence Experiments. (i) Steady-State Fluorescence Measurements. Steady-state fluorescence experiments were performed at 23 °C in a SPEX Fluorolog 2 or AMINCO Bowman 2 spectrophotometer, using an excitation wavelength of 295 nm. Emission spectra were recorded from 310 to 390 nm, and the fluorescence at 340 nm was used for evaluation of the acrylamide quenching experiments. Before the experiment, the enzymes were equilibrated in buffer containing 50 mM Tris/H_2SO_4, pH 8.0, by consecutive passage through two 1 mL Sephadex G-50 centrifuge columns. This treatment was demonstrated previously to provide an enzyme with empty catalytic sites (*22*). For the acrylamide quenching experiments, the cuvette contained 2 mL of 50 mM Tris/H_2SO_4, pH 8.0, 50−150 nM F_1, and acrylamide was added from a 6 M stock solution. The measured fluorescence intensities were corrected (*23*) for the inner filter effect due to acrylamide. When indicated, 2 mM MgATP was added (2 mM $MgSO_4$, 5 mM ATP; under these conditions, F_1 displays optimal activity). As a control, acrylamide quenching experiments were also performed using 0.5−1 μM NATA[2] as the fluorophor.

(ii) Fluorescence Lifetime Measurements. Fluorescence lifetimes were measured by time-correlated single photon counting using a pulsed laser-based instrument described in refs *24* and *25*; the excitation wavelength was 297 nm (frequency-doubled rhodamine 6G laser output), the emission wavelength 340 nm. Preparation of enzymes and experimental conditions were the same as for the steady-state fluorescence measurements, except that higher protein concentrations (200−500 nM) were used. Data analysis was performed by a nonlinear least-squares fitting procedure using 1−3 exponentials.

(iii) Evaluation of Acrylamide Quenching Experiments. The Stern−Volmer constant, K_{SV}, characterizing the dynamic component of the quenching process, was determined by nonlinear least-squares analysis of fluorescence lifetime data according to

$$\tau/\tau_0 = 1/(1 + K_{SV}[Q]) \quad (1)$$

where τ and τ_0 are the (averaged) lifetimes in the presence and in absence of quencher, respectively, and [Q] is the quencher concentration. From K_{SV} the average bimolecular quenching constant, k_q, was calculated using $k_q = K_{SV}/\langle\tau_f\rangle$, where $\langle\tau_f\rangle$ is the intensity average lifetime. Steady-state fluorescence experiments served to determine the static quenching component, V, using the equation:

$$F/F_0 = 1/[(1 + K_{SV}[Q])\cdot e^{V[Q]}] \quad (2)$$

where F and F_0 are the fluorescence intensities in the presence and in absence of quencher, respectively, and K_{SV} is the Stern−Volmer constant obtained in the lifetime experiments (*23, 26*).

RESULTS

General. In this work fluorescence properties of specifically inserted Trp residues were investigated to gain informa-

[1] *Escherichia coli* residue numbering is used throughout.

[2] Abbreviations: NATA, *N*-acetyl-L-tryptophanamide; NBD-Cl, 7-chloro-4-nitrobenz-2-oxa-1,3-diazole; K_{SV}, Stern−Volmer quenching constant; k_q, bimolecular quenching constant.

tion about the conformations of catalytic and noncatalytic sites in F_1-ATPase. For this purpose, seven Trp substitutions in the catalytic sites and one in the noncatalytic sites were chosen, based on the X-ray structure (*1*) and on our previous work (*6*). In each case the inserted Trp residue was contained in either the α- or the *β*-subunit, and since α- and *β*-subunits are present in three copies per F_1, each purified mutant enzyme contained three total Trp, all the natural Trp residues having been substituted away (see Experimental Procedures).

A brief description of the inserted Trp residues is as follows. Around the catalytic site were the following: (a) *βF148W*, which is 12 Å away from the *γ*-phosphate; the fluorescence responses of *β*-Trp-148 enabled us previously to differentiate between MgATP and MgADP bound in the catalytic sites, leading to a new model for cooperative ("multisite") MgATP hydrolysis (*2, 4, 12*); (b) *βV153W*, located between α- and *β*-phosphates of bound nucleotide (*6, 12*); (c) *βF176W*, which is located 11 Å away from the phosphate-binding pocket; this residue was newly introduced in the present study to yield a Trp residue expected to be buried and relatively inaccessible; (d) *βY331W*, where the Trp replaces a Tyr which stacks against the adenine ring of catalytic-site-bound nucleotide; using the fluorescence of *β*Y331W in F_1 and F_1F_o, we were able to quantify the pronounced functional asymmetry of the catalytic sites, to study the role of Mg^{2+} in cooperative catalysis as well as its coordination, and to investigate the structure of the catalytic transition state (*11, 22, 27*−*31*); (e) *βF410W*, which is located close to both adenine and ribose moieties (*6*); (f) α*F354W* and (g) α*F291W*, both located on the α-subunit close to the catalytic site, the former opposite the ribose moiety, the latter about 9−10 Å away from the *γ*-phosphate (*6*). In the noncatalytic sites, we studied α*R365W* (*14*). α-Arg-365 is equivalent to *β*-Tyr-331 in catalytic sites, and the aliphatic portion of the α-Arg-365 side chain abuts directly on the adenine ring of noncatalytic-site-bound nucleotide. Using the fluorescence of αR365W F_1, we demonstrated previously the symmetry of noncatalytic sites as well as the absence of a direct function in ATP hydrolysis (*14*).

All of the above mutants except *β*F176W have been described before in references cited above. All yield enzyme with normal or near-normal activity, except *β*V153W, which has a V_{max} equal to 12.5% of wild-type (*6, 12*). As stated above, the *β*F176W mutation was introduced here for the first time, and it was necessary to establish properties of this mutant enzyme before using it. Therefore, we shall briefly describe properties of *β*F176W F_1, and then describe the fluorescence experiments on the whole group of mutants.

Properties of βF176W Mutant F_1. Strain pRLL2/DK8, carrying the *β*F176W mutation, gave slightly lower than wild-type level of growth on succinate plates, and its growth yield in liquid medium containing limiting (3 mM) glucose was 80% of wild-type. These results indicated that the *β*F176W mutation caused a small impairment of normal function. *β*F176W mutant F_1 of normal molecular size and subunit composition (as judged by the elution profile of the Sephacryl S-300 gel chromatography column used in the last purification step and by SDS-gel electrophoresis) was isolated from strain pRLL2/DK8. Purified mutant enzyme exhibited a V_{max} of 25 units/mg (89% of wild-type) and a K_M of 78 *μ*M (87% of wild-type), resulting in $k_{cat}/K_M = 2.0 \times 10^6\ M^{-1}\ s^{-1}$, which is identical to wild-type. Steady-state fluorescence properties of *β*F176W mutant F_1 were as follows. The corrected emission spectrum of *β*F176W mutant F_1 exhibited a maximum at 324 nm (Figure 1, curve 1), indicating a very unpolar environment of the Trp. Addition of saturating concentrations of Mg^{2+}-nucleotide resulted in pronounced fluorescence decreases without a change of the wavelength position of the spectrum. MgADP gave 28% decrease (Figure 1, curve 2), and MgADP·fluoroberyllate complex gave 33% decrease (Figure 1, curve 3). With MgAMPPNP and MgATP, similar results were obtained. Residue *β*-Trp-176 had been chosen for inclusion in this study with the expectation that it would represent an inaccessible location close to the catalytic site (see above), and these data confirmed that this was likely to be the case.

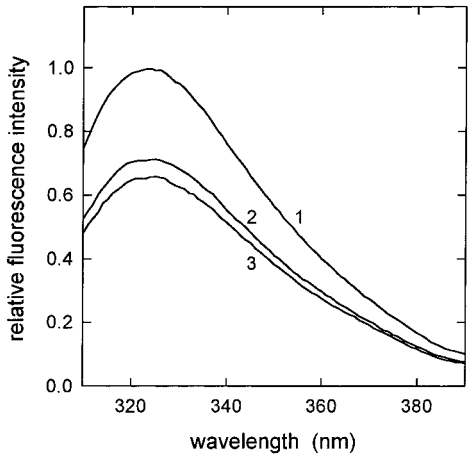

FIGURE 1: Corrected Trp fluorescence spectra of *β*F176W mutant F_1. Enzyme concentration was 100 nM in 50 mM Tris/H_2SO_4, pH 8.0. Curve 1, absence of nucleotide. Curve 2, presence of 1 mM MgADP. Curve 3, presence of MgADP·fluoroberyllate (enzyme preincubated for 30 min at 23 °C with 1 mM MgADP, 1 mM $BeSO_4$, and 5 mM NaF).

Fluorescence Lifetime Measurements. Table 1 shows the results of the fluorescence lifetime measurements of the eight Trp mutants used in this study. Whereas the fluorescence decay of the reference compound NATA could be described adequately using a single exponential ($\tau = 3.01$ ns), for all mutant enzymes 3 exponentials were required to obtain a satisfactory fit ($\chi^2 \leq 1.3$). In all mutants, the decay process with the longest lifetime accounted for ≥80% of the total fluorescence intensity. $<\tau_a>$, the amplitude average lifetime, was between 3.3 and 4.4 ns for most of the Trp residues. However, there was one clear exception, *β*-Trp-331, which had an unusually high average lifetime of close to 7 ns (*32, 33*).

Effect of Acrylamide on ATPase Activity of F_1. Acrylamide is widely used to determine accessibility of Trp residues in proteins (*26, 33*). Before the intended acrylamide quenching experiments, it was necessary to establish the upper limit of acrylamide concentration tolerated by enzyme without inactivation. Figure 2 shows ATPase activity of wild-type and Trp-free F_1 (from which all mutants used in this study are derived) as a function of acrylamide concentration. It can be seen that up to an acrylamide concentration of ∼0.6 M, ATPase activity of both enzymes actually increased, but above this concentration activity abruptly fell to zero, thus limiting the useful acrylamide concentration range for quenching studies to 0−0.5 M. The activity increase was

Table 1: Fluorescence Lifetimes of Trp Mutants[a]

mutant F_1	α_1	τ_1 (ns)	α_2	τ_2 (ns)	α_3	τ_3 (ns)	$<\tau_a>$ (ns)	$<\tau_f>$ (ns)
βF148W	0.170	0.33	0.276	2.15	0.554	4.85	3.34	4.23
βV153W	0.058	0.35	0.296	2.03	0.646	5.16	3.96	4.66
βF176W	0.032	0.23	0.205	1.79	0.763	4.43	3.75	4.17
βY331W	0.036	0.18	0.119	1.27	0.845	7.80	6.75	7.64
βF410W	0.094	0.28	0.278	1.44	0.628	4.88	3.49	4.46
αF291W	0.057	0.29	0.272	1.83	0.670	5.46	4.17	5.01
αF354W	0.057	0.46	0.345	2.31	0.597	6.02	4.41	5.32
αR365W	0.067	0.35	0.382	1.83	0.551	5.22	3.60	4.53

[a] α_i is the normalized preexponential value; τ is the fluorescence lifetime; $<\tau_a>$ is the amplitude average lifetime ($=\sum\alpha_i\tau_i$); $<\tau_f>$ is the intensity average lifetime ($=\sum\alpha_i\tau_i^2/\sum\alpha_i\tau_i$).

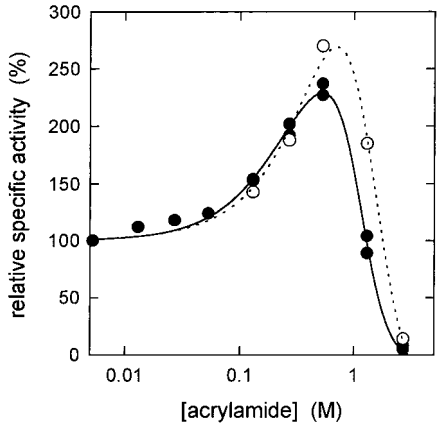

FIGURE 2: Effect of acrylamide on ATPase activity of F_1. Open circles, wild-type F_1; closed circles, Trp-free F_1. 100% corresponds to activity of 11.1 units/mg in wild-type and 17.6 units/mg in Trp-free enzyme. Details of the assay are described under Experimental Procedures.

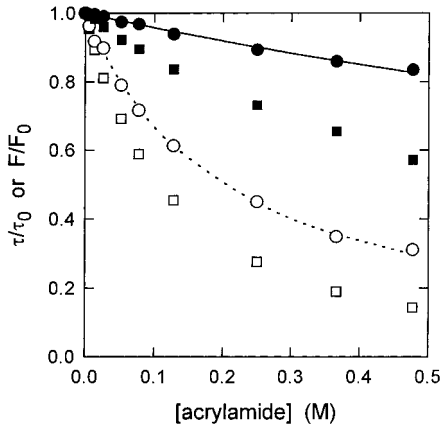

FIGURE 3: Acrylamide quenching of fluorescence of Trp mutants. The buffer was 50 mM Tris/H_2SO_4, pH 8.0. Filled symbols, βF176W mutant F_1; open symbols, βY331W mutant F_1. Circles represent τ/τ_0, the effect of acrylamide on the average fluorescence lifetime; squares represent F/F_0, the effect of acrylamide on steady-state fluorescence intensity. The lines are fits to fluorescence lifetime data using eq 1; further details are described under Experimental Procedures.

found to be due to partial dissociation of the inhibitory ϵ-subunit, since it was not observed with ϵ-depleted F_1 (data not shown). The location of ϵ (*34*), far distant from the nucleotide binding sites, makes it very unlikely that loss of this subunit affects the accessibility of the sites. Moreover, only a small fraction of the enzyme molecules is affected, since complete ϵ-depletion would result in a 10-fold activity increase (*35*).

Effect of Acrylamide on Fluorescence Lifetimes: Contribution of Dynamic Quenching. For all Trp mutants under investigation, the average fluorescence lifetime decreased as a function of increasing acrylamide concentration. Two examples, shown in Figure 3 (circles), illustrate the extreme cases. All the other mutants fell between these two. The Stern−Volmer constant, K_{SV}, was obtained by fitting theoretical curves to the measured data points, as described under Experimental Procedures. From K_{SV} we calculated the bimolecular quenching constant, k_q, which is the true measure for the susceptibility of the Trp residues to collisional quenching by acrylamide. The results are summarized in Table 2. Two Trp mutants, βY331W and βF410W, showed relatively high accessibility to acrylamide, with k_q values of 11 and 14%, respectively, of that for the model compound NATA, which is generally considered as representative of a freely accessible Trp residue in a protein. All other Trp mutants exhibited k_q values $\leq$5% of the NATA value: βF148W, 4%; βV153W, 3%; βF176W, 2%; αF291W, 3%; αF354W, 5%; αR365W, 3%. These values indicated that these Trp residues were relatively inaccessible. As will be discussed below, residue α-Trp-365 is located in the non-catalytic site, in the position equivalent to that of β-Trp-331 in the catalytic site, and the pronounced difference in accessibility between the two has important implications.

Effect of Acrylamide on Steady-State Fluorescence: Contribution of Static Quenching. Figure 3 (squares) shows data points for acrylamide quenching of steady-state fluorescence intensity of two representative Trp mutants. In all cases, quenching of the steady-state fluorescence intensity was more pronounced than the corresponding decrease in fluorescence lifetimes. This additional decrease is due to static quenching of the Trp fluorescence by acrylamide (*23*, *26*), which is described by the term V in eq 2 (see Experimental Procedures). The resulting values for V ranged from 0.25 M^{-1} in αF354W F_1 to 2 M^{-1} in βY331W F_1 and are summarized in Table 2.

Influence of MgATP on Fluorescence Lifetimes and Acrylamide Quenching. Previous measurements of nucleotide binding parameters and of K_M values had established that addition of 2 mM MgATP would result in saturation of the three catalytic binding sites with nucleotide and rapid enzyme turnover in each of the mutants. We investigated the effect of 2 mM MgATP on fluorescence decay kinetics and acrylamide quenching parameters of the Trp mutants. All four mutants, βF148W, βV153W, βF176W, and βF410W, showed moderately reduced average fluorescence lifetimes in the presence of MgATP. The changes in amplitude average lifetime ($<\tau_a>$) were −18%, −7%, −10%, and −18%,

Table 2: Acrylamide Quenching Parameters of Trp Mutants

		dynamic quenching component			static component	
mutant F_1	λ_{max}[a] (nm)	K_{SV} (M^{-1})	k_q (M^{-1} s^{-1})	MgATP effect[b] (%)	V (M^{-1})	MgATP effect[c] (%)
βF148W	328	1.00	0.235×10^9	−19	0.89	−17
βV153W	325	0.82	0.175×10^9	+6	1.25	−1
βF176W	324	0.44	0.104×10^9	+4	0.80	−27
βY331W	348	4.94	0.646×10^9	ND[d]	2.08	ND
βF410W	336[e]	3.70	0.830×10^9	−28	1.14	−85
αF291W	332	0.95	0.190×10^9	*f*	0.46	*f*
αF354W	331	1.47	0.276×10^9	*f*	0.25	*f*
αR365W	345	0.78	0.171×10^9	ND[d]	1.09	ND
NATA	353	17.4	5.77×10^9		1.63	

[a] λ_{max}, wavelength position of maximum of corrected emission spectrum. [b] % change in k_q upon addition of 2 mM MgATP. [c] % change in V upon addition of 2 mM MgATP. [d] ND, not determined; MgATP completely quenches the fluorescence signal. [e] Revised data for βF410W indicate λ_{max} = 336 nm, quench by 2 mM MgATP = 50%, λ_{max} in the presence of MgATP = 329 nm (cf. ref *6*). [f] See Results.

respectively, mostly due to a decrease in contribution of the decay process with the longest lifetime. (It should be recalled that the steady-state fluorescence intensity at 340 nm of all four of these mutants was diminished in the presence of MgATP; see above and refs *6*, *12*.) The susceptibility to dynamic quenching by acrylamide in the presence of MgATP was somewhat reduced in βF148W and βF410W F_1, but not in βV153W and βF176W enzymes (see Table 2). A protective effect of MgATP on the static quenching component was observed for β-Trp-148, β-Trp-176, and, especially, β-Trp-410 (Table 2).

Investigation of effects of MgATP on fluorescence lifetimes and acrylamide quenching was not possible with βY331W nor with αR365W F_1, since the nucleotide totally quenches the fluorescence of the introduced Trp in these cases (*14*, *27*). With αF291W and αF354W, no influence of MgATP on acrylamide quenching of the steady-state fluorescence was seen, suggesting that neither dynamic nor static quenching was occurring. Thus, the effect of MgATP on the dynamic quenching component was not investigated.

Effect of Mg^{2+} on Acrylamide Quenching of β-Trp-331 Fluorescence. Using the fluorescence signal of the βY331W mutant F_1, we earlier demonstrated that the pronounced functional asymmetry of the three catalytic sites, manifested as highly cooperative binding of nucleotide substrate MgATP or product MgADP, is only seen in the presence of Mg^{2+}. In the absence of Mg^{2+}, i.e., with uncomplexed ATP or ADP, the sites behave symmetrically (*2*, *22*). It was of interest therefore to find out whether the three β-Trp-331 residues themselves behaved asymmetrically in the presence of Mg^{2+}, which would indicate an asymmetry in catalytic sites unoccupied by nucleotide. We therefore investigated the effect of 2.5 mM $MgSO_4$ on acrylamide quenching of βY331W F_1 fluorescence using lifetime measurements.

The presence of Mg^{2+} alone, in the absence of acrylamide, had no significant effect on the decay kinetics. In either the presence or absence of Mg^{2+}, eq 1 (see Experimental Procedures) was found sufficient to describe the quenching behavior in the presence of acrylamide. Figure 4 shows the results (in the presence of Mg^{2+}) plotted in the form of the traditional Stern−Volmer plot (where $\tau_0/\tau = 1 + K_{SV}[Q]$). The solid line is a fit to the data points assuming a single K_{SV} value, and the fit is seen to be excellent. The calculated quenching parameters were $K_{SV} = 4.67$ M^{-1} and $k_q = 0.612 \times 10^9$ M^{-1} s^{-1}, similar to the values found in the absence of Mg^{2+} in Table 2.

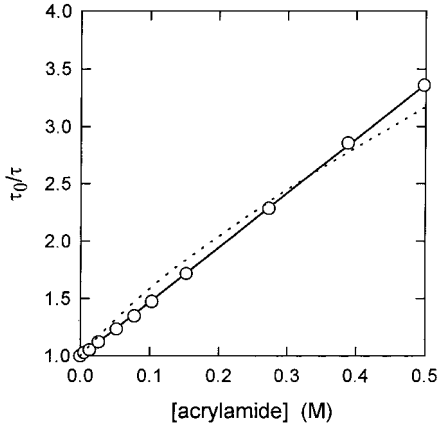

FIGURE 4: Acrylamide quenching of βY331W mutant F_1 fluorescence in the presence of Mg^{2+}. Enzyme concentration was 350 nM in 50 mM Tris/H_2SO_4, pH 8.0, 2.5 mM $MgSO_4$. The solid line is a fit to the data points assuming a single K_{SV} (k_q) value for each of the three β-Trp-331 residues. The dotted line uses an asymmetric model in which one of the three sites has a k_q value corresponding to that of α-Trp-365 (see Discussion).

DISCUSSION

General. The goal of this study was a more comprehensive analysis of the fluorescence properties of eight mutant *Escherichia coli* F_1-ATPases, seven with a specifically engineered Trp in the environment of the three catalytic sites, and one with a Trp inserted in the adenine-binding subdomain of the three noncatalytic sites.[3] In all cases, the inserted Trp residues are the only tryptophans in the enzyme. The fluorescence parameters investigated were the decay kinetics and the susceptibility to acrylamide quenching.

Fluorescence Lifetime Measurements. The lifetime measurements showed that the fluorescence decay for all eight of the inserted Trp residues could be described adequately by three exponentials (Table 1). Multiexponential decay is the rule for Trp residues in proteins (*32*, *33*), and three lifetimes have been reported (*36*) even for crystalline single-Trp proteins. Thus, the fact that each mutant enzyme investigated here actually contains three Trp residues (one per α- or β-subunit) does not appear to cause an unusually complicated decay pattern. Therefore, in general, in each enzyme all three Trp showed similar behavior, although it

[3] All eight residues which were replaced by Trp in this study are highly conserved, and present in all published X-ray structures of F_1 or $\alpha_3\beta_3$ complex.

should be noted that small variations in the decay kinetics between the three Trp residues would not have been detected by this technique.

In the specific case of β-Trp-331, this result has particular significance. The fluorescence signal of the βY331W enzyme has been used extensively to determine nucleotide binding parameters of catalytic sites of *E. coli* F_1 and F_1F_o (summarized in refs *2, 4, 5*), and is likely to find wide use in the future (e.g., refs *37, 38*). For evaluation of nucleotide binding parameters, the assumption is made that the fluorescence signal of each of the three β-Trp-331 residues is the same. There is no doubt that this is the case in the presence of nucleotide, where the signal is essentially zero at all three sites. However, the question of the contribution of each β-Trp-331 residue to the overall signal in the absence of nucleotide is important. In this work, fluorescence lifetime measurements showed that 98% of the steady-state fluorescence intensity of βY331W F_1 is associated with a decay process which has an unusually long lifetime, with no indications for any pronounced variation between the three Trp residues. It should be emphasized that only pronounced differences between the three residues would have an impact on the results of nucleotide binding analyses. Other arguments also support the idea of equal contribution of the three β-Trp-331 residues to the overall signal, namely, (i) independent site-occupancy measurements using the fluorescent nucleotide analogue lin-benzo-ADP (*22*), and (ii) the fact that modification of βY331W F_1 by NBD-Cl reduced fluorescence quenching upon addition of 1 mM MgATP (sufficient to fill all three catalytic sites in the unmodified enzyme) by exactly one-third (*22*). This is in excellent agreement with the X-ray structure of mitochondrial F_1 reacted with NBD-Cl (*39*), which shows that NBD-Cl modifies just one of the catalytic sites, preventing it from closing and binding nucleotide.

Fluorescence Quenching by Acrylamide: Discussion of Accessibility of Individual Catalytic Site Residues. Quenching by acrylamide was analyzed in terms of dynamic and static components (Table 2). The dynamic quenching component (characterized by k_q) describes the accessibility of the fluorophore Trp to collisions with the quencher, and the static component (represented by *V*) is believed to be due to the presence of quencher molecules in the direct environment of the fluorophor at the moment of excitation. It was also pertinent to compare the accessibility of the Trp residues toward acrylamide with the wavelength position of their emission spectrum (λ_{max} is given in Table 2), which reflects the polarity of the immediate microenvironment of the fluorophore (*33, 40*). Many of the results obtained could be readily rationalized in the context of available crystal structures (*1, 7, 41*), indicating that the solution structure of the Trp mutant enzymes is very similar to the crystal structure of the wild-type enzyme.

Five of the Trp residues, present in βF148W, βV153W, βF176W, αF291W, and αF354W mutants, exhibited low accessibility toward collisional quenching ($k_q < 0.3 \times 10^9$ M^{-1} s^{-1}) and a moderately to highly unpolar environment ($\lambda_{max} = 324-332$ nm). β-Trp-176 was the least accessible residue, with the most unpolar environment, in agreement with the crystal structure (*1*) which shows residue β-Phe-176 to be buried in the protein matrix and surrounded mostly by unpolar amino acid side chains (β-Tyr-206, β-Phe-240, β-Leu-204). Residue β-153 lies within the Walker Homology A sequence (*42*), which makes direct contact with the phosphates of a catalytic site-bound nucleotide molecule, mostly via hydrogen bonds between main chain nitrogen and phosphate oxygen atoms. The side chain of β-Val-153 points away from the nucleotide, and into the protein, toward the hydrophobic β-Leu-321 (side chain), β-Ser-322 (main chain), and β-Arg-323 (side chain methylene groups) (*1*), consistent with the low λ_{max} and k_q values noted for the βV153W mutant.

The results obtained here indicated that residue β-Phe-148 is buried in the protein in an unpolar environment. This is in agreement with the crystal structure (*1*), which also shows a pronounced difference in the position of the side chain of this residue between a nucleotide-occupied and an empty β-subunit. When the catalytic site is filled, β-Phe-148 forms a sandwich-type complex with β-Phe-312, whereas in an empty site the two aromatic rings lie edge-to-edge with much less overall contact. The fluorescence results obtained with the βF148W mutant enzyme suggest that the side chain of β-Trp-148 experiences a similar prominent conformational change; especially noteworthy is the significant blue-shift of the spectrum upon nucleotide binding (λ_{max} was reduced by between 3 and 6−7 nm, depending on the nucleotide; see ref *12*). The crystal structure (*1*) shows the side chains of residues α-Phe-291 and α-Phe-354 located on the surface of the α-subunit, facing into the catalytic site. However, even in an empty catalytic site the adjacent β-subunit appears to shield both residues well from the medium, and this is consistent with their low measured accessibility to acrylamide (Table 2).

In contrast, the catalytic site mutants βY331W and βF410W were found to be quite susceptible to collisional quenching by acrylamide (Table 2). X-ray structures (*1, 7, 41*) of the empty catalytic site show one side of the β-Tyr-331 ring exposed to the medium (Figure 5A, left), whereas in a nucleotide-occupied site, the aromatic ring is stacked against the adenine ring of the nucleotide (Figure 5A, right). The fluorescence properties of βY331W F_1 suggest a similar solution structure for the Trp mutant. In nucleotide-filled sites, the β-Trp-331 fluorescence was virtually completely quenched (*13, 27*), in all likelihood due to formation of a sandwich-type complex between Trp and adenine ring systems. In empty sites, the red-shifted wavelength position of the emission spectrum ($\lambda_{max} = 348$ nm) indicates exposure to water molecules from the medium.

Residue β-410 is located on the opposite side of the adenine binding pocket from β-331. The crystal structure (*1*) indicates that residue β-Phe-410 should be freely accessible not only from the cleft, but also to some extent directly from the surrounding medium (Figure 5A), and this appears to be reflected by the high k_q value for the Trp residue in βF410W mutant F_1 (Table 2). The relatively low λ_{max} of 336 nm for such an accessible Trp residue is not without precedent, and is usually associated with restricted motion of the Trp side chain (*40*). Addition of MgATP caused a blue-shift of the emission maximum of 7 nm, and protected the fluorophore from collisional and, especially, static quenching. This reduction in accessibility is consistent with closing of the cleft upon binding of nucleotide (Figure 5A).

Fluorescence Quenching by Acrylamide: Discussion of Accessibility of Noncatalytic Site Residue α*-Trp-365.* Earlier

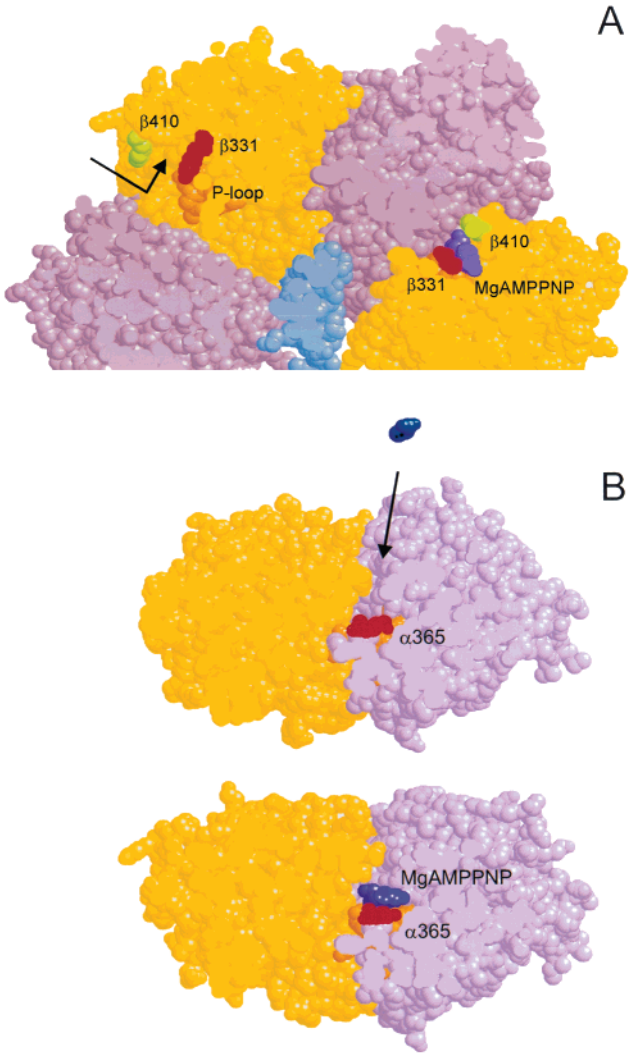

FIGURE 5: Accessibility of Trp residues from the medium. The figures are based on the crystal structures in (*1*) and (*7*) and were generated using RasMol software, kindly provided by Dr. Roger Sayle, Glaxo Research. A transverse section of the enzyme at the level of the nucleotide binding sites is shown in the bottom view, as seen from the membrane. Except for the highlighted residues, the α-subunit is shown in pink, *β* in yellow, *γ* in light blue. (A) Catalytic sites. Residues *β*-331 and *β*-410 at an empty (left) or at an occupied (right) catalytic site. Shown are the wild-type residues *β*-Tyr-331 (red) and *β*-Phe-410 (green). To facilitate orientation, the Walker A ("P-loop", ref *42*) residues are shown in orange. In the occupied site, the nucleotide is shown in purple. At the empty site, the arrow points to the adenine binding pocket (width 8−10 Å) of the nucleotide binding site, which branches off from a cleft between the α- and *β*-subunits that is about 15 Å wide at this point. This cleft is closed in the occupied site. (B) Noncatalytic sites. Residue α-365 at an empty (top) or at an occupied (bottom) noncatalytic site. The wild-type residue α-Arg-365 is shown in red, the P-loop in orange, the nucleotide in purple. The cleft between α- and *β*-subunits (arrow) is much narrower than in an empty catalytic site, impairing the accessiblility to acrylamide (blue, drawn to scale).

work (*14*) had shown that in empty noncatalytic sites the α-Trp-365 emission spectrum was strongly red-shifted (Table 2), and that the fluorescence signal was virtually completely quenched upon nucleotide binding. Thus, in several ways, α-Trp-365 in the noncatalytic sites behaves similarly to *β*-Trp-331 in the catalytic sites (residues α-365 and *β*-331 are equivalent in the sequences). In the crystal structure the relative position of the protein backbone around these residues is the same in both types of site; the methylene groups of the α-Arg-365 side chain make van der Waals contact with the adenine ring of noncatalytic site-bound nucleotide (*1, 2*). The fluorescence response indicates that the adenine ring forms a complex with the α-Trp-365 side chain which is very similar to that formed with *β*-Trp-331 in the catalytic site. Interestingly, α-Trp-365 was much less susceptible to collisional quenching by acrylamide than *β*-Trp-331; the respective k_q values differed by a factor of close to 4 (Table 2). The crystal structure of the $\alpha_3\beta_3$ subcomplex of F_1 from the thermophilic bacterium PS3 (*7*) reveals the reason for this behavior. Even when the noncatalytic sites are not occupied by nucleotide, the α-subunit is in a "closed" conformation (Figure 5B). Our fluorescence data suggest that under these conditions the nucleotide binding cleft contains water molecules; however, the access for acrylamide is largely blocked.

"Open" and "Closed" Conformations of the Catalytic Sites. Noncatalytic sites, whether empty or occupied by nucleotide, appear to take up the same "closed" conformation of the α-subunit (Figure 5B, see ref. *1, 7, 41*), leading to low accessibility to acrylamide as noted above, and also explaining the slow rates of nucleotide binding to these sites (*14*). In contrast, two main conformations of the catalytic sites have been seen: a "closed" one, when the catalytic site is occupied (*1, 41*), and an "open" one, when the catalytic site is empty (*1, 7*). It is quite possible that new, intermediate conformations will be seen as new crystal structures are solved. There is good evidence indicating that a *β*-subunit in an occupied catalytic site is always in a closed or partially closed state (*4, 43*), although this point of view has been challenged (*44*). One question is whether the *β*-subunit of an empty catalytic site in intact F_1 is always in an open conformation. Whereas the crystal structure of the $\alpha_3\beta_3$ subcomplex (*7*) suggests that this might indeed be the case (all three catalytic sites are empty, and all three *β*-subunits are open), it is also possible that this pattern is the consequence of the lack of the central *γ*-subunit (*44*).

Results presented in this study show that in intact F_1, when all three catalytic sites are empty, all three *β*-Trp-331 residues are relatively and equally accessible to acrylamide, in marked contrast to α-Trp-365 in an empty noncatalytic site on a closed α-subunit. To demonstrate this point, we have included in Figure 4 (dashed line) a fit where the k_q value for one of the three *β*-Trp-331 residues was held constant at the value determined for α-Trp-365 to resemble a closed conformation, and only k_q for the remaining two sites was allowed to iterate. It is obvious that the resulting fit is worse than that assuming three identical quenching constants. It should be noted that this result was obtained even in the presence of Mg^{2+} (Figure 4), which is a prerequisite for functional asymmetry between the three catalytic sites. The data strongly support the conclusion that when a catalytic site is unoccupied, it assumes, in time average, an open conformation. Other support for this conclusion comes from the kinetic data for Mg-nucleotide binding, which show that all three catalytic sites bind Mg-nucleotide with rapid and approximately equal on-rates (*2*). In (*44*) it was concluded from Cys−Cys cross-linking studies that $\alpha_3\beta_3\gamma$ complex with unoccupied catalytic sites exists with two sites in the closed and one site in the open conformation. Possibly, random fluctuations of the protein may close the catalytic sites from

time to time, leading to their being trapped in the closed conformation by the cross-linking procedure, which therefore would not give a true view of the predominant time average conformation.

ACKNOWLEDGMENT

We thank Drs. Christopher J. Collison and Stephen J. Atherton of the NSF Center for Photoinduced Charge Transfer (Department of Chemistry, University of Rochester) for their invaluable help with the fluorescence lifetime measurements. We also thank Rachael Laundry, Rachel Shaner and Christine Schaner for excellent technical assistance.

REFERENCES

1. Abrahams, J. P., Leslie, A. G. W., Lutter, R., and Walker, J. E. (1994) *Nature 370*, 621−628.
2. Weber, J., and Senior, A. E. (1997) *Biochim. Biophys. Acta 1319*, 19−58.
3. Nakamoto, R. K., Ketchum, C. J., and Al-Shawi, M. K. (1999) *Annu. Rev. Biophys. Biomol. Struct. 28*, 205−234.
4. Weber, J., and Senior, A. E. (2000) *Biochim. Biophys. Acta* (in press).
5. Senior, A. E., Nadanaciva, S., and Weber, J. (2000) *J. Exp. Biol. 203*, 35−40.
6. Weber, J., Wilke-Mounts, S., Hammond, S. T., and Senior, A. E. (1998) *Biochemistry 37*, 12042−12050.
7. Shirakihara, Y., Leslie, A. G. W., Abrahams, J. P., Walker, J. E., Ueda, T., Sekimoto, Y., Kambara, M., Saika, K., Kagawa, Y., and Yoshida, M. (1997) *Structure 5*, 825−836.
8. Vandeyar, M., Weiner, M., Hutton, C., and Batt, C. (1988) *Gene 65*, 129−133.
9. Wilke-Mounts, S., Weber, J., Grell, E., and Senior, A. E. (1994) *Arch. Biochem. Biophys. 309*, 363−368.
10. Ketchum, C. J., Al-Shawi, M. K., and Nakamoto, R. K. (1998) *Biochem. J. 330*, 707−712.
11. Nadanaciva, S., Weber, J., and Senior, A. E. (1999) *Biochemistry 38*, 7670−7677.
12. Weber, J., Bowman, C., and Senior, A. E. (1996) *J. Biol. Chem. 271*, 18711−18718.
13. Weber, J., and Senior, A. E. (1995) *J. Biol. Chem. 270*, 12653−12658.
14. Weber, J., Wilke-Mounts, S., Grell, E., and Senior, A. E. (1994) *J. Biol. Chem. 269*, 11261−11268.
15. Weber, J., Lee, R. S. F., Grell, E., Wise, J. G., and Senior, A. E. (1992) *J. Biol. Chem. 267*, 1712−1718.
16. Senior, A. E., Lee, R. S. F., Al-Shawi, M. K., and Weber, J. (1992) *Arch. Biochem. Biophys. 297*, 340−344
17. Laemmli, U. K. (1970) *Nature 227*, 680−685.
18. Bradford, M. M. (1976) *Anal. Biochem. 72*, 248−254.
19. Senior, A. E., Latchney, L. R., Ferguson, A. M., and Wise, J. G. (1984) *Arch. Biochem. Biophys. 228*, 49−53.
20. Taussky, H. H., and Shorr, E. (1953) *J. Biol. Chem. 202*, 675−685.
21. van Veldhoven, P. P., and Mannaerts, G. P. (1987) *Anal. Biochem. 161*, 45−48.
22. Weber, J., Wilke-Mounts, S., and Senior, A. E. (1994) *J. Biol. Chem. 269*, 20462−20467.
23. Lakowicz, J. R. (1983) *Principles of Fluorescence Spectroscopy*, Plenum Press, New York.
24. Chen, H., Farahat, M. S., Law, K. Y., and Whitten, D. G. (1996) *J. Am. Chem. Soc. 118*, 2584−2594.
25. Arnold, B. R., Atherton, S. J., Farid, S., Goodman, J. L., and Gould, I. R. (1997) *Photochem. Photobiol. 65*, 15−22.
26. Eftink, M. R., and Ghiron, C. A. (1976) *Biochemistry 15*, 672−680.
27. Weber, J., Wilke-Mounts, S., Lee, R. S. F., Grell, E., and Senior, A. E. (1993) *J. Biol. Chem. 268*, 20126−20133.
28. Weber, J., Hammond, S. T., Wilke-Mounts, S., and Senior, A. E. (1998) *Biochemistry 37*, 608−614.
29. Löbau, S., Weber, J., and Senior, A. E. (1998) *Biochemistry 37*, 10846−10853.
30. Nadanaciva, S., Weber, J., and Senior, A. E. (1999) *J. Biol. Chem. 274*, 7052−7058.
31. Nadanaciva, S., Weber, J., Wilke-Mounts, S., and Senior, A. E. (1999) *Biochemistry 38*, 15493−15499.
32. Beechem, J. M., and Brand, L. (1985) *Annu. Rev. Biochem. 54*, 43−71.
33. Eftink, M. R. (1991) *Methods Biochem. Anal. 35*, 127−205.
34. Stock, D., Leslie, A. G. W., and Walker, J. E. (1999) *Science 286*, 1700−1705.
35. Weber, J., Dunn, S. D., and Senior, A. E. (1999) *J. Biol. Chem. 274*, 19124−19128.
36. Dahms, T. E. S., and Szabo, A. G. (1997) *Methods Enzymol. 278*, 202−221.
37. Grüber, G., and Capaldi, R. A. (1996) *J. Biol. Chem. 271*, 32623−32628.
38. Dou, C., Fortes, G,. and Allison W. S. (1998) *Biochemistry 37*, 16757−16764.
39. Orriss, G. L., Leslie, A. G. W., Braig, K., and Walker, J. E. (1998) *Structure 6*, 831−837.
40. Callis, P. R. (1997) *Methods Enzymol. 278*, 113−150.
41. Bianchet, M. A., Hullihen, J., Pedersen, P. L., and Amzel, L. M. (1998) *Proc. Natl. Acad. Sci. U.S.A. 95*, 11065−11070.
42. Walker, J. E., Saraste, M., Runswick, M. J., and Gay, N. J. (1982) *EMBO J. 1*, 945−951.
43. Yagi, H., Tozawa, K., Sekino, N., Iwabuchi, T., Yoshida, M., and Akutsu, H. (1999) *Biophys. J. 77*, 2175−2183.
44. Ren, H., Dou, C., Stelzer, M. S., and Allison, W. S. (1999) *J. Biol. Chem. 274*, 31366−31372.

BI992730T